

Modeling wave dark matter in dwarf spheroidal galaxies

H L Bray¹ and A R Parry²

¹Department of Mathematics and Department of Physics, Duke University, Box 90320, Durham, NC 27708, USA

²Department of Mathematics, University of Connecticut, 196 Auditorium Road, Unit 3009, Storrs, CT 06269, USA

E-mail: ¹bray@math.duke.edu, ²alan.parry@uconn.edu

Abstract. This paper studies a model of dark matter called wave dark matter (also known as scalar field dark matter and boson stars). Wave dark matter describes dark matter as a scalar field which satisfies the Einstein-Klein-Gordon equations. These equations rely on a fundamental constant Υ (also known as the “mass term” of the Klein-Gordon equation), which can be interpreted physically as a characteristic frequency of the scalar field. In this work, we compare the wave dark matter model to observations to obtain an estimate of Υ . Specifically, we compare the mass profiles of spherically symmetric static states of wave dark matter to certain Burkert mass profiles recently shown to predict well the velocity dispersion profiles of the eight classical dwarf spheroidal galaxies. We outline a procedure for estimating Υ in these circumstances and show that under precise assumptions the value of Υ can be bounded above by 1000 yr^{-1} . We also show that a reasonable working value for this constant is $\Upsilon = 50 \text{ yr}^{-1}$.

1. Introduction

Ever since the first postulation of dark matter in the 1930's by Oort [1] and then Zwicky [2], much evidence for the existence of dark matter has been accumulated including the unexpected behavior in the rotation curves of spiral galaxies [3, 4], the velocity dispersion profiles of dwarf spheroidal galaxies [5, 6, 7, 8], and gravitational lensing [9]. These and other observations support the idea that most of the matter in the universe is not baryonic, but is, in fact, some form of exotic dark matter and that almost all astronomical objects from the galactic scale up contain a significant amount of this dark matter. Describing dark matter, its nature, and effects is currently one of the biggest open problems in astrophysics [10, 11, 12, 13, 14, 15, 16].

Essentially all of the observations indicating the presence of dark matter are gravitational observations, that is, we have only observed the gravitational effects of dark matter. Since, from the point of view of general relativity, gravity is an effect of the curvature of spacetime, this indicates that, when it comes to dark matter, what is being observed is some kind of unexplained curvature of the spacetime. This suggests the possibility that the key to understanding the nature of dark matter already lies within the framework of general relativity. Recently, Bray has geometrically motivated the study of a scalar field satisfying the Einstein-Klein-Gordon equations as a viable dark matter candidate via constructing axioms for general relativity [17, 18]. This geometric motivation shows that modeling dark matter with a scalar field is perhaps the most natural large scale point of view for the dark matter problem.



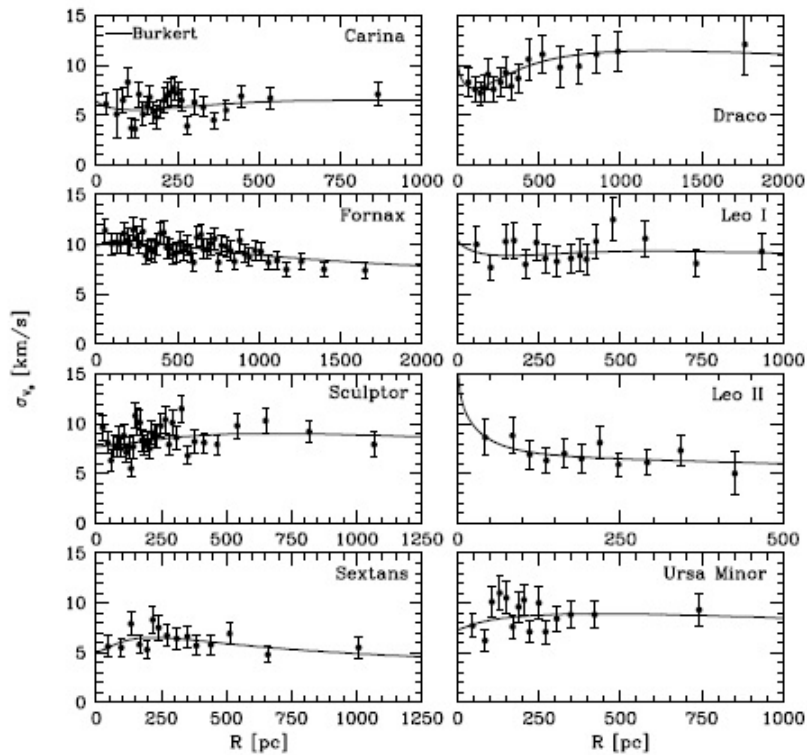


Figure 1. Observed velocity dispersion profiles of the eight classical dwarf spheroidal galaxies are denoted by the points on each plot with its associated error bars. The solid lines overlaid on these profiles are the best fit velocity dispersion profiles induced by the Burkert mass profile. This figure is directly reproduced from Figure 1 of the paper “Dwarf spheroidal galaxy kinematics and spiral galaxy scaling laws” by Salucci et al. appearing in the Monthly Notices of the Royal Astronomical Society volume 420 issue 3 [6]. The reader is referred to their paper for a complete description of how these models were computed.

The idea of using a scalar field to describe dark matter is not new. In fact, a scalar field model has been seriously considered as a candidate for dark matter for more than two decades and has been shown to be in agreement with many cosmological observations [17, 19, 20, 21, 22, 23, 24, 25, 26, 27, 28, 29, 30, 31]. In most of these settings, these scalar fields are considered from a quantum mechanical motivation for the same Einstein-Klein-Gordon equations and go by the name scalar field dark matter or boson stars. However, due to the fact that the Klein-Gordon equation is a wave-type partial differential equation, we prefer the name *wave dark matter* and will refer to the scalar field model as such in the remainder of this paper.

Specifically, wave dark matter is characterized by a single scalar field permeating all of a spacetime (N, g) whose metric g has signature $(-+++)$. The scalar field, which is either a real or complex-valued function, and the metric together form a solution to the Einstein-Klein-Gordon equations. In this paper, we consider the point of view of a complex-valued scalar

field $f : N \rightarrow \mathbb{C}$. In this case, the Einstein-Klein-Gordon equations are given by

$$G = 8\pi\mu_0 \left(\frac{df \otimes d\bar{f} + d\bar{f} \otimes df}{\Upsilon^2} - \left(\frac{|df|^2}{\Upsilon^2} + |f|^2 \right) g \right) \quad (1a)$$

$$\square_g f = \Upsilon^2 f \quad (1b)$$

where \square_g is the Laplacian with respect to the metric g , and $\mu_0 \geq 0$ and $\Upsilon > 0$ are constants. The constant μ_0 is for convenience and is related to the value of the energy density of the scalar field at the origin. If desired, μ_0 can be completely absorbed into f and hence its value does not affect the solutions qualitatively. However, Υ is a fundamental constant of this system and its value affects the qualitative behavior of the solutions. Physically, Υ can be interpreted as a characteristic frequency of the scalar field. From a particle physics point of view, the constant Υ is related to the mass m^* of the dark matter particle. Specifically,

$$m^* = \frac{\hbar\Upsilon}{c} = 2.09 \times 10^{-23} \text{ eV} \left(\frac{\Upsilon}{1 \text{ yr}^{-1}} \right) \quad (2)$$

In the wave dark matter model, the value of Υ is the same throughout all of spacetime since the scalar field permeates all of spacetime, making Υ a fundamental constant of the universe. Thus an important check for the validity of this model is to see if a single constant value of Υ can successfully describe all of the observed gravitational effects of dark matter in all contexts. Moreover, we can use observations of dark matter in any context to bound this parameter since its value is the same everywhere. This is positive since the more estimates of Υ that we can obtain, the more clearly we will be able to determine if this model is valid.

One of the simplest models defined by wave dark matter are the spherically symmetric static states. These models are well known and are sometimes referred to as standing waves of the Einstein-Klein-Gordon equations. These models are shown by Parry in [32] to have certain useful properties. These properties, in fact, present an opportunity to estimate Υ . The purpose of this paper is to use these properties of spherically symmetric static states and recent observations of dwarf spheroidal galaxies to provide an estimate of and bounds on Υ . Additionally, this paper gives support to the notion that a single value of Υ is sufficient to describe dark matter at all levels by showing that a single value is at least sufficient to describe the dark matter content in the dwarf spheroidal galaxies considered here and that, in fact, many values work in this case.

In particular, Salucci et al. recently used the cored Burkert profile [33] to model the dark matter energy density profiles of the eight classical dwarf spheroidal galaxies orbiting the Milky Way. They found excellent agreement between the observed velocity dispersion profiles of these galaxies and those velocity dispersion profiles induced by the Burkert profile [6]. This can be seen in Figure 1, which we have reproduced exactly as it appears in the paper by Salucci et al. In what follows, we will use the properties of spherically symmetric static states of wave dark matter to show that under precise assumptions, comparisons to these Burkert profiles can be used to bound the value of Υ above by 1000 yr^{-1} . We will also show that a value of $\Upsilon = 50 \text{ yr}^{-1}$ produces wave dark matter mass models that are qualitatively similar to the Burkert mass models found by Salucci et al. as an example that a single value of Υ can be used to describe the dark matter mass content of all of the dwarf spheroidal galaxies considered here.

2. Burkert Mass Profiles

The Burkert energy density profile models the energy density of a spherically symmetric dark matter halo using the function

$$\mu_B(r) = \frac{\rho_0 r_c^3}{(r + r_c)(r^2 + r_c^2)} \quad (3)$$

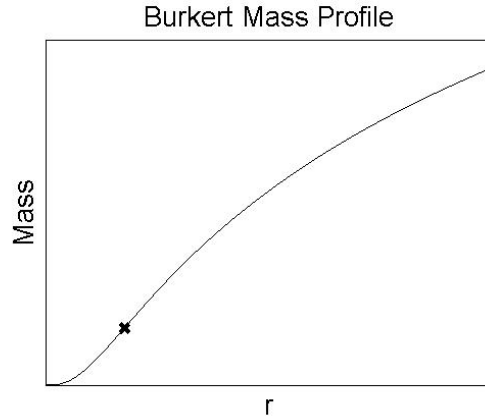


Figure 2. Plot of a Burkert mass profile. The inflection point is marked with an \times .

where ρ_0 is the central density and r_c is the core radius. Integrating this function over the ball of radius r centered at the origin, $B_r(0)$, with respect to the standard spherical volume form yields the Burkert mass profile as follows.

$$\begin{aligned}
 M_B(r) &= \int_{B_r(0)} \mu_B(s) dV_{\mathbb{R}^3} \\
 &= 4\pi \int_0^r s^2 \mu_B(s) ds \\
 &= 4\pi \int_0^r \frac{s^2 \rho_0 r_c^3}{(s+r_c)(s^2+r_c^2)} ds \\
 M_B(r) &= 2\pi \rho_0 r_c^3 \left(\ln \left(\frac{r+r_c}{r_c} \right) \right. \\
 &\quad \left. + \frac{1}{2} \ln \left(\frac{r^2+r_c^2}{r_c^2} \right) - \arctan \left(\frac{r}{r_c} \right) \right) \tag{4}
 \end{aligned}$$

A generic plot of a Burkert mass profile, $M_B(r)$, defined to be the dark matter mass in the ball of radius r , is shown in Figure 2. We make a few remarks about the behavior of this mass function.

Note that the behavior of the graph changes concavity at the inflection point $r = r_{ip}$, which we have marked on the plot in Figure 2 with an \times . Recalling from equation (4) the fact that $M_B(r)$ is the integral over the interval $[0, r]$ of the function $4\pi r^2 \mu_B(r)$, we can compute this inflection point as follows.

$$M'_B(r) = 4\pi r^2 \mu_B(r) = \frac{4\pi \rho_0 r_c^3 r^2}{(r+r_c)(r^2+r_c^2)} \tag{5}$$

Differentiating again yields

$$M''_B(r) = \frac{-4\pi \rho_0 r_c^3 (r^4 - r^2 r_c^2 - 2r r_c^3)}{(r+r_c)^2 (r^2+r_c^2)^2}, \tag{6}$$

which has two complex zeros and two real zeros. The two real zeros are $r = 0$ and

$$r_{ip} = \left(\frac{3 + (27 + 3\sqrt{78})^{2/3}}{3(27 + 3\sqrt{78})^{1/3}} \right) r_c \approx 1.52 r_c, \tag{7}$$

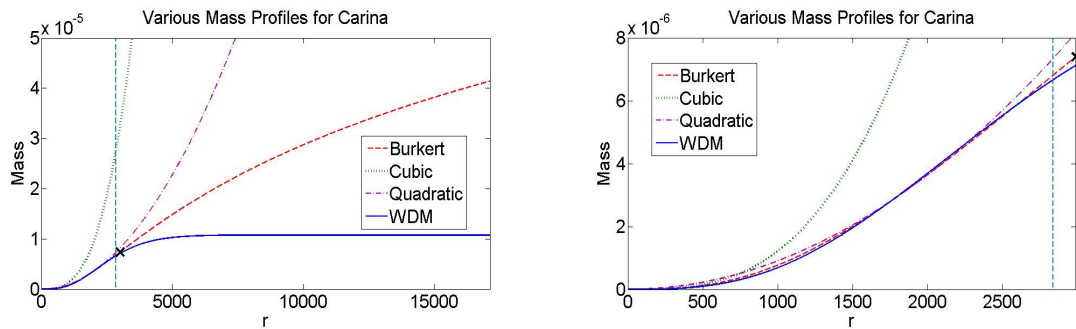


Figure 3. Left: Plot of the Burkert mass profile for the Carina galaxy found by Salucci et al. [6] along with a mass plot of a wave dark matter static ground state, the cubic function which is the leading term of the Taylor expansion of the Burkert mass profile, and the quadratic power function $\frac{M_B(r_c)}{r_c^2} r^2$ where r_c is the core radius of the Carina galaxy. The \times marks the location of the inflection point of the Burkert mass profile, while the vertical line denotes the location of the outermost data point for the Carina galaxy and is presented for reference purposes only. Right: Closeup of the plot on the left over the r interval $[0, r_{ip}]$.

the latter being the inflection point of the mass model.

For $r \gg r_{ip}$, the plot grows logarithmically due to the fact that the arctan term in equation (4) approaches a constant value as $r \rightarrow \infty$. To describe the behavior when $r \ll r_{ip}$, we note that the Taylor expansion of $M_B(r)$ centered at $r = 0$ is as follows,

$$M_B(r) = \frac{4}{3} \pi \rho_0 r^3 + O(r^4). \quad (8)$$

Thus for $r \ll r_{ip}$, $M_B(r)$ is dominated by an r^3 term making the initial behavior cubic.

In fact, several other models for dark matter mass profiles have similar initial behavior to the Burkert profile including a quadratic mass profile (which is not physical and is only included for the sake of comparison) and wave dark matter mass profiles. In Figure 3, we have collected several mass models that have similar behavior inside $r = r_{ip}$ to the Burkert mass profile computed by Salucci et al. for the Carina galaxy [6]. While these models have similar behavior inside $r = r_{ip}$, they are very different outside $r = r_{ip}$.

We have computed the inflection points of each of the Burkert mass profiles computed by Salucci et al. for the eight classical dwarf spheroidal galaxies [6] and have marked these points on a plot of each Burkert mass profile in Figure 4. We have constrained the viewing window of each plot to the range of data points collected. That is, we plot the Burkert mass profiles on the interval $[0, r_{last}]$, where r_{last} is the radius of the outermost data point given by Walker et al. [7, 8] for the observed velocity dispersion profiles. We have presented them in order from greatest to least according to the ratio of r_{last}/r_{ip} .

In Table 1, we have collected the defining parameters, ρ_0 and r_c , computed by Salucci et al. for the Burkert mass profiles which best predict the velocity dispersion profiles of each galaxy [6]. We have also collected the outermost data point, r_{last} , of these velocity dispersion profiles [7, 8], as well as our computations of the inflection point, r_{ip} , and the ratio r_{last}/r_{ip} for each of the classical dwarf spheroidal galaxies. All quantities have been converted to geometrized units (the universal gravitational constant and the speed of light set to one) of (light)years for mass, length, and time.

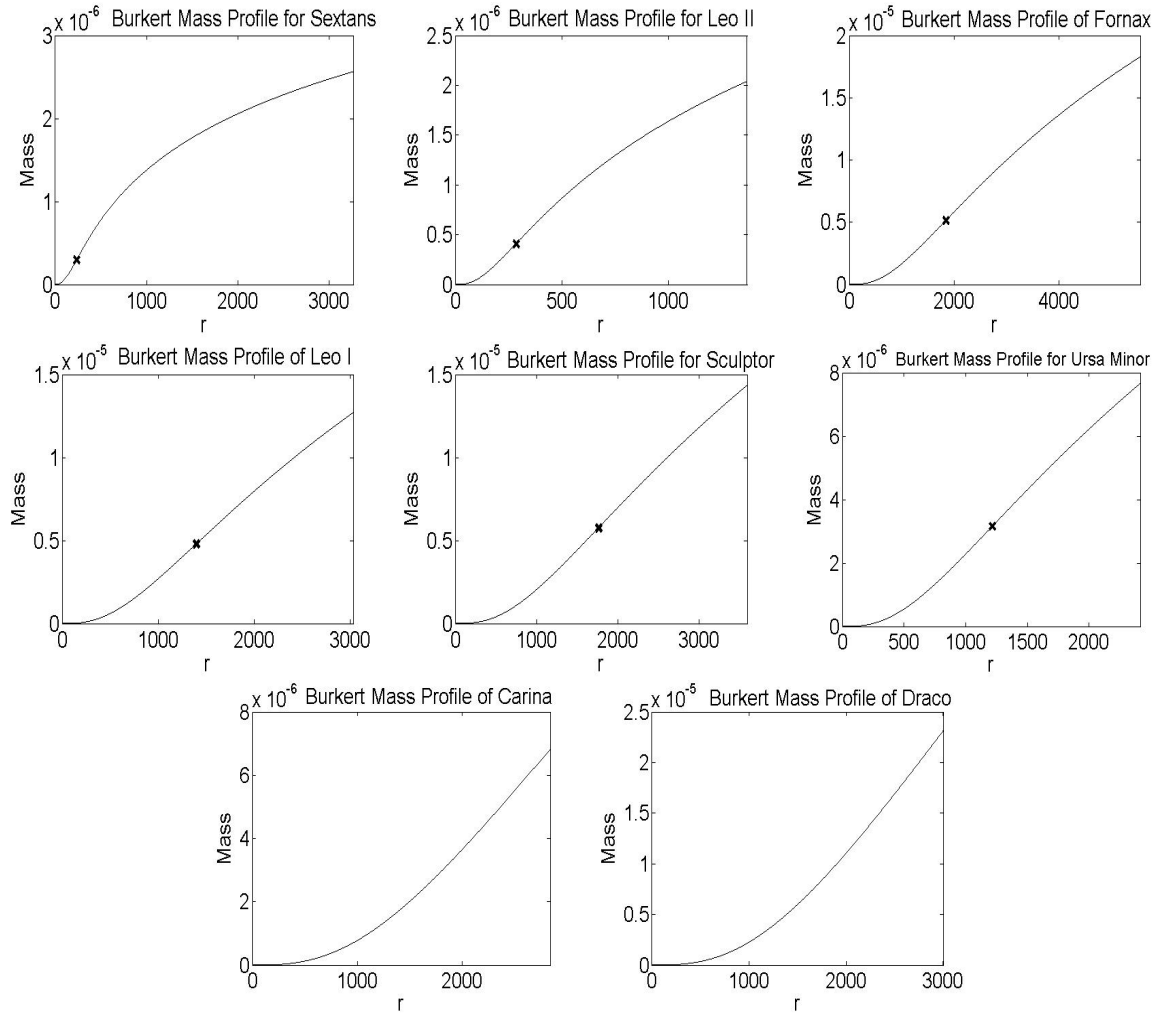


Figure 4. Plots of the Burkert mass profiles computed by Salucci et al. of the eight classical dwarf spheroidal galaxies within the range of observable data. The inflection point is marked on each plot by an \times . Carina and Draco have no inflection point marked because the inflection point for their Burkert mass profiles occurs outside the range of observable data.

3. Static States of Wave Dark Matter

Now that we have presented mass profiles which model actual data well, we need to describe the wave dark matter models we will use to make our comparison. In the following, we present only the basic background information required to understand the model we use and refer the reader to [17, 18] for more discussion on its motivation and successes thus far.

Since we wish to compare solutions of (1) to the spherically symmetric Burkert mass profiles computed by Salucci et al. [6], we choose to work in spherical symmetry. In [34], Parry surveyed the well-known form of the metric of a general spherically symmetric spacetime in polar-areaal coordinates, namely,

$$g = -e^{2V(t,r)} dt^2 + \left(1 - \frac{2M(t,r)}{r}\right)^{-1} dr^2 + r^2 d\sigma^2, \quad (9)$$

for real valued functions V and M and where $d\sigma^2 = d\theta^2 + \sin^2\theta d\varphi^2$ is the standard metric

Galaxy Name	ρ_0 (yr ⁻²)	r_c (yr)	r_{last} (yr)	r_{ip} (yr)	r_{last}/r_{ip}
Sextans	2.47×10^{-14}	1.53×10^2	3.26×10^3	2.32×10^2	14.05
Leo II	1.83×10^{-14}	1.88×10^2	1.37×10^3	2.86×10^2	4.80
Fornax	8.57×10^{-16}	1.21×10^3	5.54×10^3	1.84×10^3	3.01
Leo I	1.83×10^{-15}	9.19×10^2	3.03×10^3	1.40×10^3	2.17
Sculptor	1.10×10^{-15}	1.16×10^3	3.59×10^3	1.76×10^3	2.04
Ursa Minor	1.83×10^{-15}	8.01×10^2	2.41×10^3	1.22×10^3	1.98
Carina	2.90×10^{-16}	1.97×10^3	2.84×10^3	2.99×10^3	0.95
Draco	8.19×10^{-16}	2.11×10^3	3.00×10^3	3.20×10^3	0.94

Table 1. Burkert mass profile data for the eight classical dwarf spheroidal galaxies converted to units of years for mass, length, and time. The parameters ρ_0 and r_c are those found by Salucci et al. for the best fit Burkert profiles [6], and r_{last} is the radius of the outermost data point given by Walker et al. [7, 8]. Also included is the value of the inflection point, r_{ip} , of the Burkert mass profile for each galaxy and the ratio of r_{last} to r_{ip} .

on the unit sphere. This metric has the following useful properties. The function $M(t, r)$ is the Hawking mass of the metric sphere of radius r and time t . Under the Einstein equation, $G = 8\pi T$, M is also the flat volume integral of the energy density term in the stress energy tensor. This motivates interpreting the function $M(t, r)$ as the mass inside the metric sphere of radius r at time t . Finally, given the Einstein equation, in the low field limit, V is approximately the gravitational potential of the system. We refer the reader to [34] for detailed proofs of these facts.

It is also shown in [34] that in spherical symmetry and using the metric (9), solving the Einstein-Klein-Gordon system (1) reduces to solving the system

$$M_r = 4\pi r^2 \mu_0 \left(|f|^2 + \left(1 - \frac{2M}{r}\right) \frac{|f_r|^2 + |p|^2}{\Upsilon^2} \right) \quad (10a)$$

$$V_r = \left(1 - \frac{2M}{r}\right)^{-1} \left(\frac{M}{r^2} - 4\pi r \mu_0 \left(|f|^2 - \left(1 - \frac{2M}{r}\right) \frac{|f_r|^2 + |p|^2}{\Upsilon^2} \right) \right) \quad (10b)$$

$$f_t = p e^V \sqrt{1 - \frac{2M}{r}} \quad (10c)$$

$$p_t = e^V \left(-\Upsilon^2 f \left(1 - \frac{2M}{r}\right)^{-1/2} + \frac{2f_r}{r} \sqrt{1 - \frac{2M}{r}} \right) + \partial_r \left(e^V f_r \sqrt{1 - \frac{2M}{r}} \right). \quad (10d)$$

To solve this system, we need boundary conditions. At the central value, we require all of the functions to be smooth. Since all of the functions are spherically symmetric, this implies that M_r , V_r , f_r , and p_r all vanish at $r = 0$ for all t . We will also require that the spacetime be asymptotically Schwarzschild, that is, it approaches a Schwarzschild metric as $r \rightarrow \infty$.

Specifically, this implies that

$$e^{2V} \rightarrow \kappa^2 \left(1 - \frac{2M}{r}\right) \quad \text{as } r \rightarrow \infty \quad (11)$$

$$\square_{g_S} f \rightarrow \Upsilon^2 f \quad \text{and} \quad f \rightarrow 0 \quad \text{as } r \rightarrow \infty \quad (12)$$

where $\kappa > 0$ and g_S is the appropriate Schwarzschild metric. Since $f \rightarrow 0$ as $r \rightarrow \infty$, M approaches a constant value m , which is the total mass of the system.

Note that these boundary conditions ensure that as $r \rightarrow \infty$, the metric g in equation (9) becomes the Schwarzschild metric

$$g_S = -\kappa^2 \left(1 - \frac{2m}{r}\right) dt^2 + \left(1 - \frac{2m}{r}\right)^{-1} dr^2 + r^2 d\sigma^2. \quad (13)$$

Thus κ represents a scaling of the t coordinate in the standard Schwarzschild metric. The effect of this on our discussion is that $V \rightarrow \ln \kappa$ as $r \rightarrow \infty$.

We have to numerically solve these equations and so in practice, we will impose these boundary conditions at an artificial right hand boundary point r_{max} and solve the system on the r -interval $[0, r_{max}]$.

One of the simplest solutions to this system are those where the scalar field is of the form

$$f(t, r) = e^{i\omega t} F(r) \quad (14)$$

where $\omega \in \mathbb{R}$ is a constant and F is real valued.

Note that for f of this form, solving equation (12) for large r and requiring the solution to decay to 0 yields that, for large r and small total mass, F must satisfy

$$F' + \left(\sqrt{\Upsilon^2 - \frac{\omega^2}{\kappa^2}} + \frac{1}{r}\right) F \approx 0. \quad (15)$$

Requiring this condition on our system ensures that f appropriately decays to 0 as $r \rightarrow \infty$. See [35] for more details on this computation.

Solutions of the form in equation (14) produce static metrics and, once substituted into the system (10), yield the following set of ODEs [32],

$$M' = 4\pi r^2 \mu_0 \left[\left(1 + \frac{\omega^2}{\Upsilon^2} e^{-2V}\right) |F|^2 + \left(1 - \frac{2M}{r}\right) \frac{|H|^2}{\Upsilon^2} \right] \quad (16a)$$

$$V' = \left(1 - \frac{2M}{r}\right)^{-1} \left\{ \frac{M}{r^2} - 4\pi r \mu_0 \left[\left(1 - \frac{\omega^2}{\Upsilon^2} e^{-2V}\right) |F|^2 - \left(1 - \frac{2M}{r}\right) \frac{|H|^2}{\Upsilon^2} \right] \right\} \quad (16b)$$

$$F' = H \quad (16c)$$

$$H' = \left(1 - \frac{2M}{r}\right)^{-1} \left[\left(\Upsilon^2 - \frac{\omega^2}{e^{2V}}\right) F + 2H \left(\frac{M}{r^2} + 4\pi r \mu_0 |F|^2 - \frac{1}{r}\right) \right] \quad (16d)$$

with boundary conditions

$$F(0) = 1, \quad H(0) = 0, \quad M(0) = 0, \quad V(0) = V_0, \quad (17)$$

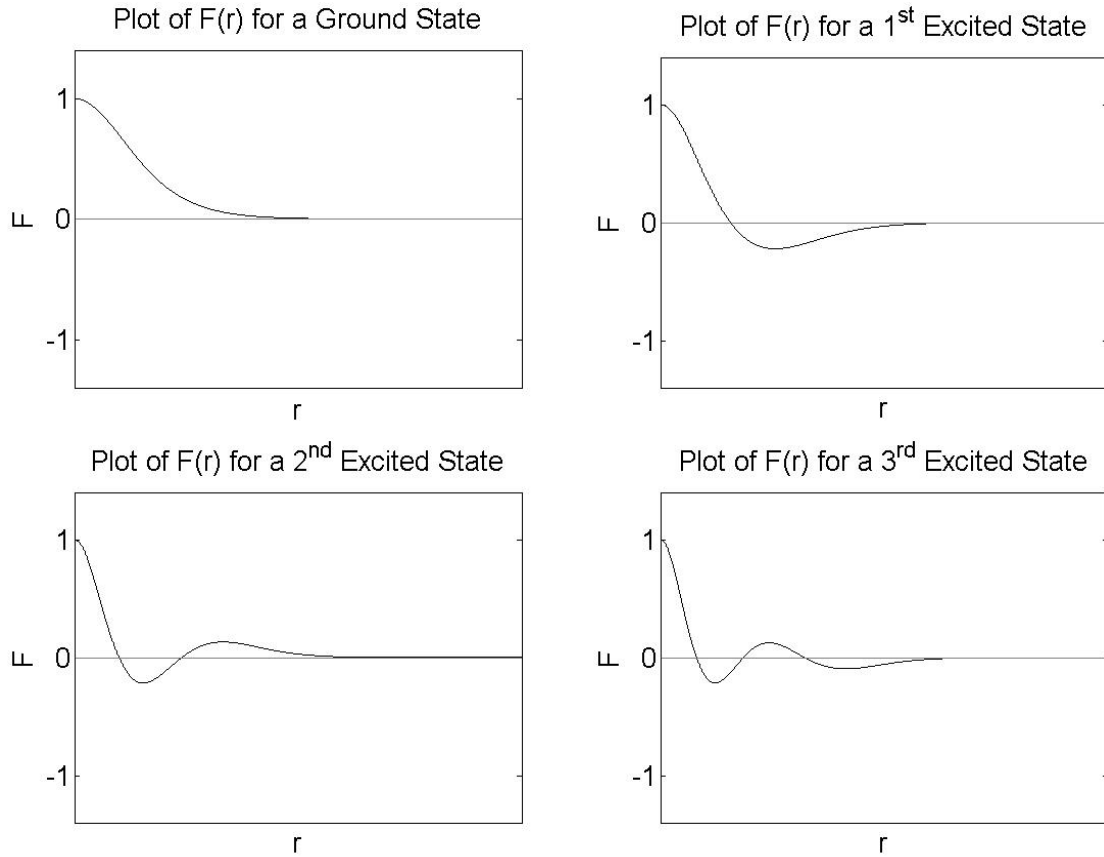


Figure 5. Plots of spherically symmetric static state scalar fields (specifically, the function $F(r)$ in equation (14)) in the ground state and first, second, and third excited states. Note the number of nodes (zeros) of each function.

$$F'(r_{max}) + \left(\sqrt{\Upsilon^2 - \frac{\omega^2}{\kappa^2}} + \frac{1}{r_{max}} \right) F(r_{max}) \approx 0, \quad (18)$$

$$V(r_{max}) - \frac{1}{2} \ln \left(1 - \frac{2M(r_{max})}{r_{max}} \right) - \ln \kappa \approx 0, \quad (19)$$

by equations (11) and (12). For simplicity, we set $\kappa = 1$, which corresponds to the assumption on our choice of t coordinate that V goes to zero at infinity and that the metric goes to the standard Schwarzschild metric as $r \rightarrow \infty$. A solution to these equations depends on the choice of the parameters Υ , μ_0 , ω , and V_0 . We solve a shooting problem for ω and V_0 to satisfy (18) and (19) leaving Υ and μ_0 freely selectable.

For each choice of Υ and μ_0 , there are an infinite number of discrete finite mass solutions characterized by the number of zeros that F exhibits [32, 36]. These are called static states. A static state with no zeros is called a ground state. With n zeros for $n > 0$, it is called an n^{th} excited state. In Figure 5, we have plotted examples of F for a ground through third excited state. In Figure 6, we have presented the plots of the mass, M , corresponding to the plots of F in Figure 5.

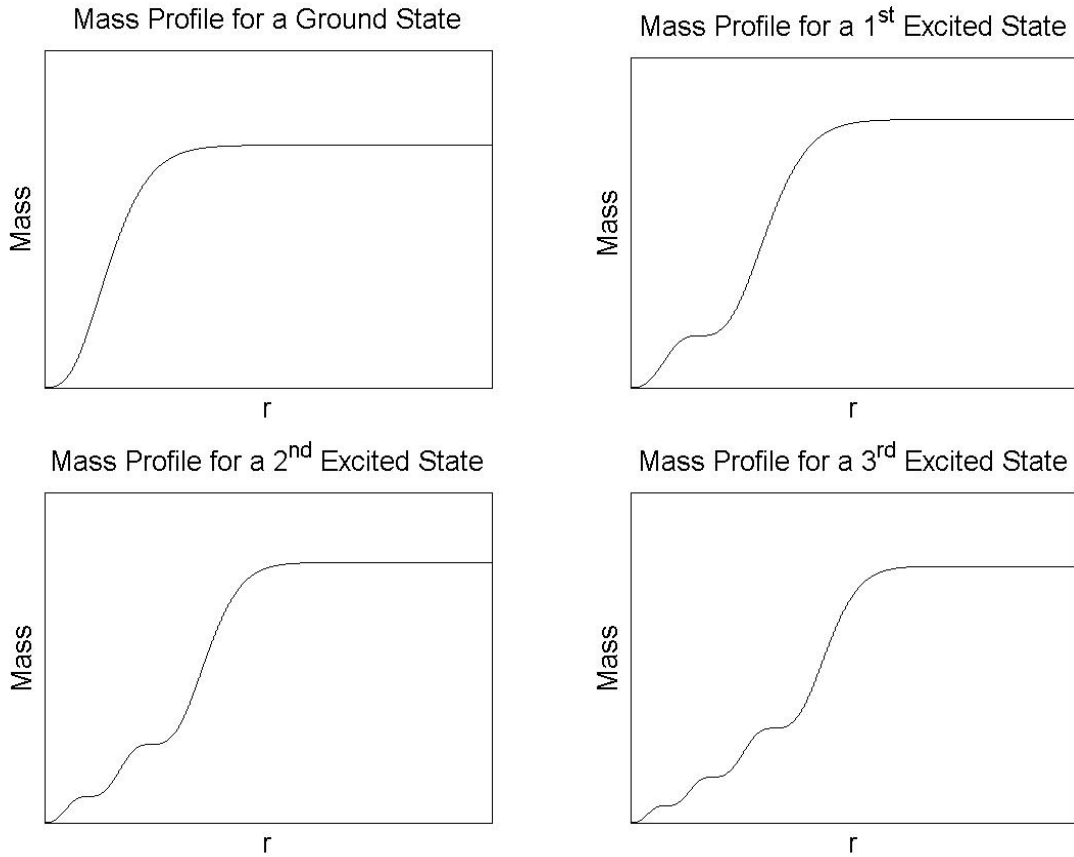


Figure 6. Mass profiles for a static ground state and first, second, and third excited states of wave dark matter.

3.1. Hyperbolas of Constant Υ

Parry showed in [32] how the parameters which define an n^{th} excited state, Υ , μ_0 , ω , and V_0 , as well as the values of the total mass, m , and the radius, r_h , called the half mass radius, for which $M(r_h) = m/2$, are related to each other. The approximations which follow only apply to solutions in the long wavelength, low field limit, which is what is relevant for modeling galaxies. In particular, for constant Υ , there is a one parameter family of solutions for each n^{th} excited state defined by the equations

$$\omega^n(\Upsilon, \mu_0) \approx \Upsilon \exp\left(C_{frequency}^n \frac{\sqrt{\mu_0}}{\Upsilon}\right) \quad (20)$$

$$V_0^n(\Upsilon, \mu_0) \approx C_{potential}^n \frac{\sqrt{\mu_0}}{\Upsilon} \quad (21)$$

$$m^n(\Upsilon, \mu_0) \approx C_{mass}^n \Upsilon^{-3/2} \mu_0^{1/4} \quad (22)$$

$$r_h^n(\Upsilon, \mu_0) \approx C_{radius}^n \Upsilon^{-1/2} \mu_0^{-1/4}. \quad (23)$$

where the constants C_*^n depend upon which state we wish to consider (i.e. they depend on n). Thus for constant Υ , the different possible excited states satisfying equations (17), (18), and (19) are defined entirely by the value of μ_0 , which corresponds to the value of the energy density

n	C_{mass}^n	C_{radius}^n
0	4.567 ± 0.05	0.8462 ± 0.004
1	10.22 ± 0.10	2.2894 ± 0.009
2	15.81 ± 0.16	3.8253 ± 0.014
3	21.37 ± 0.22	5.3994 ± 0.018
4	26.91 ± 0.27	6.9860 ± 0.022
5	32.42 ± 0.33	8.5606 ± 0.026
10	60.32 ± 1.18	15.1357 ± 0.039
20	116.62 ± 2.57	29.6822 ± 0.107

Table 2. Values of the constants in equations (22) and (23) for the ground through fifth excited states as well as the tenth and twentieth excited states. We have given these values error ranges which encompass the interval we observed in our experiments, but it is possible that values outside our ranges here could be observed. However, we do not expect them to be outside by much if the discretization of r used in solving the ODEs is sufficiently fine. Note also that our values have less precision as we increase n . This is because as n increases, it becomes more difficult to compute the states with as much precision.

function, μ , as defined in [34] at the origin via the equation

$$\mu(0) = \mu_0 \left(1 + \frac{\omega^2}{\Upsilon^2} e^{-2V_0} \right). \quad (24)$$

The equations relevant to our discussion here are equations (22) and (23). We have collected the values of C_{mass}^n and C_{radius}^n from these two equations for the ground through fifth excited states as well as for the tenth and twentieth excited states in Table 2. A complete table of the values of all the constants C_*^n for these excited states can be found in [32].

As explained in [32], equations (22) and (23) imply that the product of m and r_h does not depend on the value of μ_0 , but only on Υ . Specifically,

$$mr_h = \frac{C_{mass} C_{radius}}{\Upsilon^2}, \quad (25)$$

where we have suppressed the notation of n . If Υ is constant, then, because both C_{mass} and C_{radius} are positive, the right hand side of this equation is some positive constant, k , and we have

$$mr_h = k \quad (26)$$

which defines a hyperbola. Thus, for a given n^{th} excited state, all of the possible mass profiles for a constant value of Υ lie along a hyperbola. We illustrate this phenomenon in Figure 7.

3.2. Fitting Burkert Mass Profiles

With these properties of static state mass profiles in mind, we turn our attention to finding static state mass profiles that best fit the Burkert mass profiles computed by Salucci et al. [6]. Given a Burkert mass profile, M_B , a value for Υ , and a specific state (i.e. value for n), we define for our purposes the best fit wave dark matter static state mass profile, M_W , as the one which minimizes the L^2 norm of the difference between these profiles, E , given by

$$E = \|M_B - M_W\|_{L^2}^2 = \int_0^{r_{last}} (M_B - M_W)^2 dr. \quad (27)$$

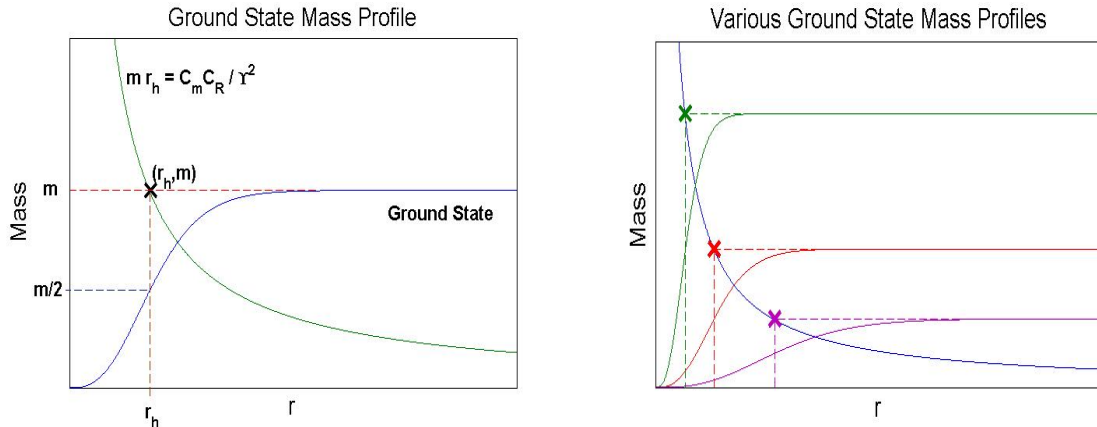


Figure 7. Left: Plot of the mass profile of a ground state with its corresponding hyperbola of constant Υ overlaid. Any ground state mass profile that keeps the presented relationship with this hyperbola corresponds to the same value of Υ . Right: Examples of different ground state mass profiles corresponding to the same value of Υ . The corresponding hyperbola of constant Υ is overlaid. Notice that all three mass profiles have the same relationship with the hyperbola.

Of course, since we compute the static states numerically, we have to approximate this norm by an appropriate Riemann sum defined on a discretization of the interval $[0, r_{last}]$.

To find this minimum, we first note that since Υ is fixed, we can write the total mass m and the value of μ_0 in terms of a choice of r_h via equations (25) and (23) respectively. Thus, we parameterize the different mass profiles of constant Υ , and hence E by r_h , that is, $E = E(r_h)$. Furthermore, since all of the static state mass profiles of constant Υ lie on a hyperbola, there will be a value of r_h that yields the minimum of $E(r_h)$.

To make computing the best fits more uniform from galaxy to galaxy, we make the choice $r_h = b r_c$, where $b > 0$ and r_c is the core radius of the Burkert profile we wish to match, and vary the free parameter b . To compute which value of b produces a minimum value of $E(r_h)$, we create a grid of r_h values around an initial choice of b of the form $[(b - step)r_c, b r_c, (b + step)r_c]$ for some $step > 0$. Next we compute $E(r_h)$ for each of the values of r_h and shift the grid, if necessary, so that it is centered on the r_h value which yielded the smallest value of $E(r_h)$. If the grid shifts, we recompute $E(r_h)$ on the new grid and continue to shift, if necessary. Once the minimum $E(r_h)$ value occurs at the center of the grid, we keep that point as the center, but cut the step size in half. We then run this shifting procedure again for this smaller grid until the minimum is at the center and then we shrink again. We continue to shrink the step size until we get to a predetermined terminal value. We generally would run the procedure until the step size was less than or equal to 2^{-10} .

This best fitting procedure provides a method of finding values of Υ , for Υ sufficiently large, which produce untenable matches to the Burkert profiles of Salucci et al. [6]. This is the topic of the next section.

3.3. Upper Bound for Υ

To find an upper bound for Υ , we first need to explain how the static states change as Υ gets large. Equation (25) implies that for a given n^{th} excited state, as Υ increases, the product $m r_h$ decreases. The hyperbolas corresponding to smaller values of $m r_h$ are those that lie closer to the mass and radius axes.

Now consider the n^{th} excited state mass profile that is the best fit to a Burkert mass profile

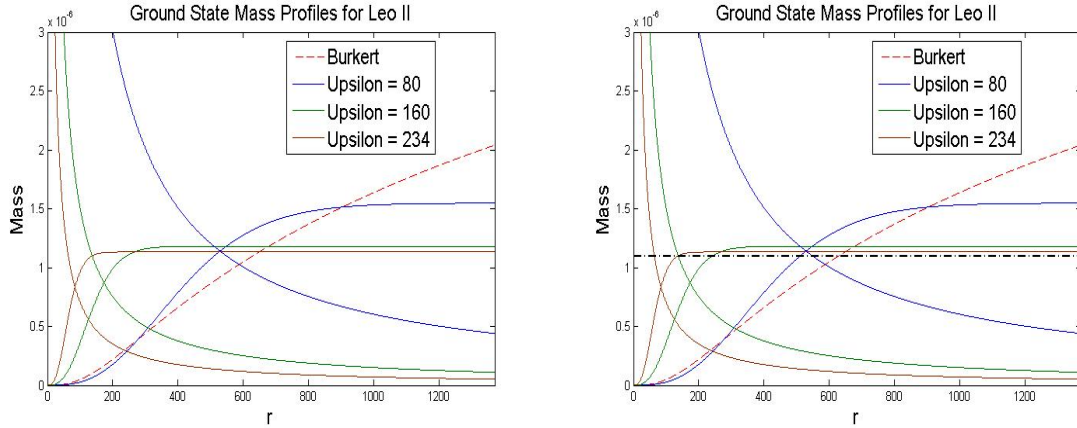


Figure 8. Left: Ground state mass profiles of various values of Υ that are best fits to the Burkert mass profile found by Salucci et al. [6] for the Leo II galaxy. The corresponding hyperbolas of constant Υ on which these profiles lie are also plotted. Ground states and their corresponding hyperbolas are drawn in the same color. Right: The same plots as in the left frame, but with the constant function which best fits the Burkert profile also plotted. Note that the best fit mass profiles approach this constant mass profile as Υ increases.

for a given Υ . As Υ increases, the hyperbola to which this static state mass profile corresponds will get closer to the mass and radius axes, but since the mass profile must also minimize $E(r_h)$, the value of its total mass will not tend to 0. Since mr_h tends to zero as $\Upsilon \rightarrow \infty$, it must be instead that $r_h \rightarrow 0$ as $\Upsilon \rightarrow \infty$. This implies that, as Υ increases, more of the constant portion of the best fitting n^{th} excited state mass profile will be compared to the Burkert profile. Thus, as $\Upsilon \rightarrow \infty$, the best fitting n^{th} excited state mass profile will limit to the constant function of r that best fits the Burkert profile under the same fitting criteria used for the static states. We illustrate this phenomenon in Figure 8.

As $\Upsilon \rightarrow \infty$, the initial increasing region (i.e. the region before the constant portion) of the n^{th} excited state mass profile that best fits a Burkert mass profile becomes more compressed. This initial region is where all of the dark matter mass is located. Thus as Υ increases, the dark matter corresponding to the best fit n^{th} excited state extends out to smaller radii. However, observations suggests that dwarf spheroidal galaxies are dark matter dominated at all observable radii [37]. Thus the best fit n^{th} excited state mass profiles for large Υ do not represent observations well and can be rejected. The question then is exactly when should we reject them.

Since every static state has the initial increasing region just described, the best fit n^{th} excited state for any value of Υ will be a better fit than the best fit constant function. Moreover, since this initial region becomes more compressed as $\Upsilon \rightarrow \infty$, for large Υ , the value of $E(r_h)$ for the best fit n^{th} excited state mass profile increases monotonically as $\Upsilon \rightarrow \infty$ approaching the value of E for the best fitting constant function.

This suggests a criteria for when to reject values of Υ . We will reject a best fit n^{th} excited state mass profile, and hence its corresponding value of Υ , as an untenable model of the dark matter mass if its value of $E(r_h)$ is greater than some prescribed fraction of the value of E for the best fitting constant function. We choose to use 80%. Explicitly, we use the following rejection criteria.

Rejection Criteria 3.1 *Given Υ , n , and a Burkert mass profile M_B , let M_W be the spherically symmetric n^{th} excited state mass profile corresponding to Υ that best fits M_B , that is, that minimizes E from equation (27) along the hyperbola defined by the value of Υ and equation*

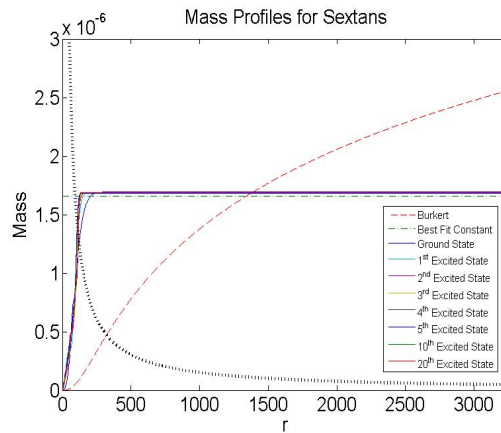


Figure 9. The Burkert mass profile found by Salucci et al. [6] for the Sextans galaxy. The best fit static state mass profiles for a ground through fifth excited state, tenth excited state, and twentieth excited state all lying on the same hyperbola are overlaid on the plot. The hyperbola here satisfies the rejection criteria for all of the different static states represented in the plot, thus all of these static states correspond to an upper bound on the value of Υ for Sextans for their respective value of n (i.e. the set of n^{th} excited states). Note how close together all of the states are. This is due to the fact that the majority of their profiles which are being compared to the Burkert mass profile is the common and constant portion of the profiles.

(25). Let E_W be the value of E for this mass profile. Furthermore, let M_C be the constant function which best fits M_B , also by minimizing the corresponding function E , and let E_C be the value of E for the constant function. Reject the given value Υ as a tenable value for this fundamental constant if

$$E_W \geq .8E_C.$$

In other words, any fit that is less than 20% better than the best fitting constant function of r is rejected as a bad fit.

For each of the eight classical dwarf spheroidal galaxies and $n \in \{0, 1, 2, 3, 4, 5, 10, 20\}$, we computed values of Υ that yielded n^{th} excited state mass profiles that best fit that galaxy's Burkert profile which were rejected by the above criteria. All of the values of Υ above those computed are also rejected because they produce mass profiles even closer to the constant function. In Table 3, we have collected these upper bounds of Υ . In Figure 9, for the galaxy Sextans, we present best fit static state mass profiles for the ground through fifth, tenth, and twentieth excited states for which $E(r_h)$ is more than 80% of the value of E for the best fit constant function.

We observe from Table 3 that the upper bound values of Υ increase as we increase the state we consider. This is due to the following. The rejected values of Υ correspond to rejected hyperbolas of constant Υ , and hence constant mr_h . Furthermore, the only qualitative difference between any two n^{th} excited state mass profiles is the number of ripples in the initial increasing region of the profile. For large Υ , the majority of a best fit n^{th} excited state mass profile that is compared to the Burkert profile is the constant region which is shared by static state mass profiles for any n . Thus the hyperbola corresponding to a rejected best fit ground state is close to the hyperbola corresponding to a rejected best fit n^{th} excited state for any n . In particular, there is a hyperbola of constant mr_h , for which the corresponding best fit n^{th} excited state mass profiles for any n are rejected by the above criteria. Then, since C_{mass}^n and C_{radius}^n appear to monotonically increase as n increases (see Table 2), by equation (25), we would expect the same

Galaxy \ State	0	1	2	3
Sextans	$\Upsilon < 160$	$\Upsilon < 394$	$\Upsilon < 633$	$\Upsilon < 875$
Leo II	$\Upsilon < 234$	$\Upsilon < 576$	$\Upsilon < 926$	$\Upsilon < 1279$
Fornax	$\Upsilon < 35$	$\Upsilon < 87$	$\Upsilon < 139$	$\Upsilon < 192$
Leo I	$\Upsilon < 57$	$\Upsilon < 141$	$\Upsilon < 226$	$\Upsilon < 312$
Sculptor	$\Upsilon < 49$	$\Upsilon < 121$	$\Upsilon < 194$	$\Upsilon < 268$
Ursa Minor	$\Upsilon < 82$	$\Upsilon < 202$	$\Upsilon < 325$	$\Upsilon < 449$
Carina	$\Upsilon < 84$	$\Upsilon < 207$	$\Upsilon < 333$	$\Upsilon < 459$
Draco	$\Upsilon < 45$	$\Upsilon < 111$	$\Upsilon < 179$	$\Upsilon < 246$

Galaxy \ State	4	5	10	20
Sextans	$\Upsilon < 1116$	$\Upsilon < 1356$	$\Upsilon < 2460$	$\Upsilon < 4789$
Leo II	$\Upsilon < 1632$	$\Upsilon < 1983$	$\Upsilon < 3597$	$\Upsilon < 7003$
Fornax	$\Upsilon < 245$	$\Upsilon < 297$	$\Upsilon < 538$	$\Upsilon < 1048$
Leo I	$\Upsilon < 398$	$\Upsilon < 484$	$\Upsilon < 877$	$\Upsilon < 1706$
Sculptor	$\Upsilon < 342$	$\Upsilon < 416$	$\Upsilon < 754$	$\Upsilon < 1467$
Ursa Minor	$\Upsilon < 572$	$\Upsilon < 695$	$\Upsilon < 1261$	$\Upsilon < 2455$
Carina	$\Upsilon < 586$	$\Upsilon < 712$	$\Upsilon < 1292$	$\Upsilon < 2514$
Draco	$\Upsilon < 314$	$\Upsilon < 382$	$\Upsilon < 692$	$\Upsilon < 1347$

Table 3. Upper bound values for Υ corresponding to poor best fits of the Burkert mass profiles for each of the classic dwarf spheroidal galaxies. The values in each column for each galaxy should be interpreted as an upper bound on the value of Υ , under the approximations explained in the paper, if that galaxy is best modeled by an n^{th} excited state. The units on Υ are yr^{-1} .

behavior for the value of Υ in order for mr_h to remain constant, which is what we observe in Table 3.

Thus if a dwarf spheroidal galaxy is correctly modeled by a twentieth excited state or less, then an overall upper bound on the value of Υ would be the upper bound corresponding to the twentieth excited state. The least upper bound corresponding to the twentieth excited state over all eight galaxies is that value for the Fornax galaxy, which yields approximately that

$$\Upsilon < 1000 \text{ yr}^{-1}. \quad (28)$$

3.4. Working Value of Υ

The last objective of this paper is to provide an example of a single value of Υ being qualitatively consistent with the dark matter mass profiles of each of the eight classical dwarf spheroidal galaxies. As shown in the last section, all of the values $\Upsilon < 1000$ are such examples to varying levels of tolerance. In this section, we present an example where the qualitative similarity is readily apparent.

For $\Upsilon = 50 \text{ yr}^{-1}$, there is at least one wave dark matter static state mass profile, which is a third excited state or less, for each of the Burkert mass profiles of the eight classical dwarf spheroidal galaxies that matches reasonably well. We have plotted such matches in Figure 10. Due to the fact that these mass profiles match reasonably well, we will use

$$\Upsilon = 50 \text{ yr}^{-1} \quad (29)$$

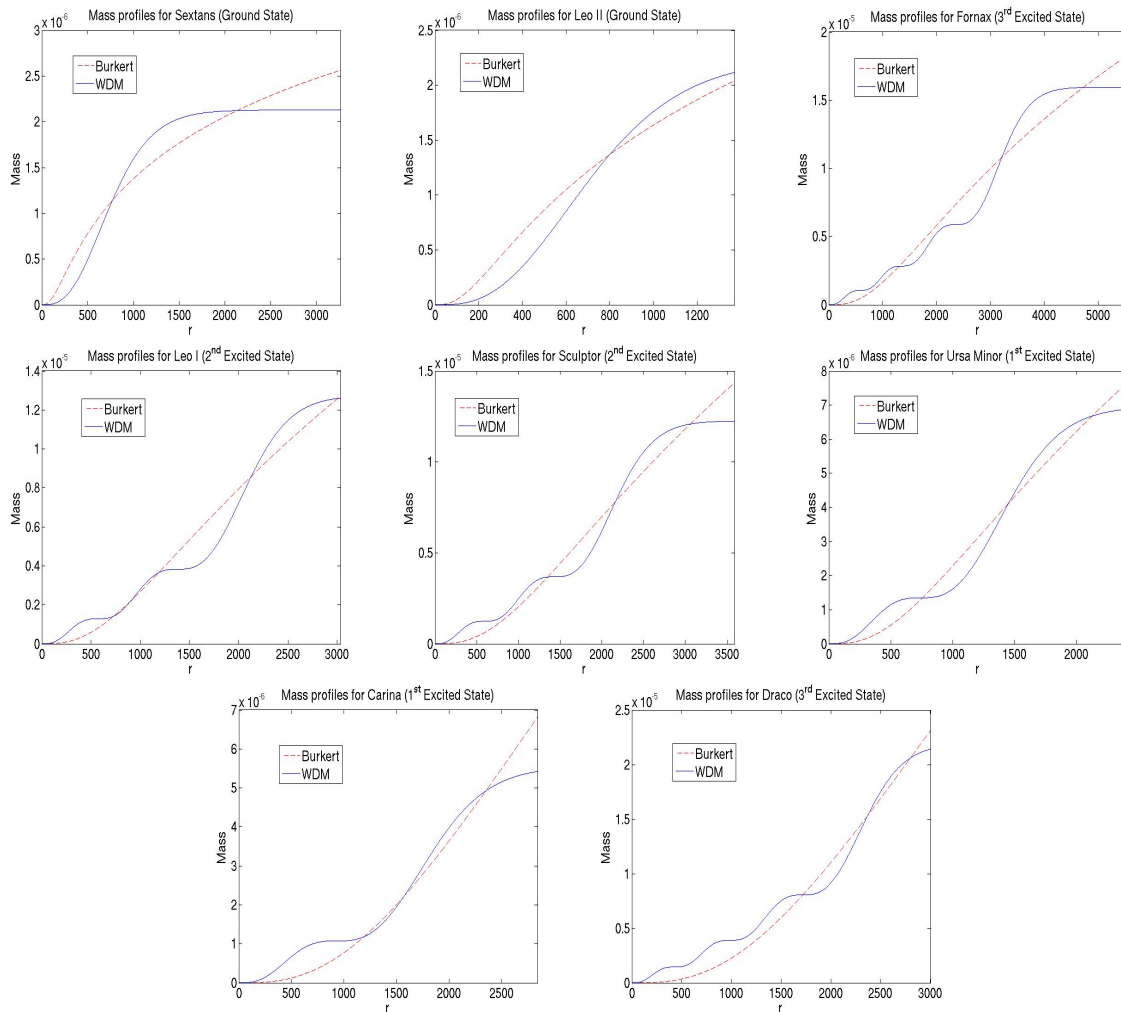


Figure 10. Static state mass profiles for $\Upsilon = 50$ which are each a best fit to the Burkert profiles of the corresponding dwarf spheroidal galaxy. For $\Upsilon = 50$, we picked an n^{th} excited state whose best fit profile matched the Burkert profile qualitatively well. This shows that $\Upsilon = 50$ is a reasonable working value of Υ . However, it does not imply that the actual value of Υ is 50 or that these galaxies are correctly modeled by the presented n^{th} excited state. The units on Υ are yr^{-1} .

as a working value of Υ in our future work with wave dark matter until we have the capability to make a more accurate approximation or precise measurement of this value.

While we have chosen $\Upsilon = 50 \text{ yr}^{-1}$ as a working value of Υ since it corresponds to wave dark matter models compatible with other well fitting models, we note that the above does not constitute a precise measurement of the value of Υ . As said before, this is merely an example that a single value of Υ is sufficient to produce dark matter mass profiles that are qualitatively similar to the profiles found by Salucci et al.

4. Utilized Approximations

Now that we have presented our results, we list here the important approximations made in this paper which led to these results and explain briefly why we make them.

Approximation 1: Dark matter is correctly described by the wave dark matter model.

Approximation 2: Dark matter halos around dwarf spheroidal galaxies are spherically symmetric.

Approximation 3: The dwarf spheroidal galaxies used in this paper are in a state of dynamical equilibrium.

Approximation 4: The spacetime metrics describing these dwarf spheroidal galaxies are static.

Approximation 5: Wave dark matter predicts outcomes qualitatively similar to those of spherically symmetric static state solutions to the Einstein-Klein-Gordon equations.

Approximation 6: The Burkert mass profiles computed by Salucci et al. [6] fit the observational data very well.

Approximation 7: The spacetime is in the low field limit, that is, $M \ll r$.

Approximation 8: The spacetime is asymptotically Schwarzschild.

Approximation 1 is used because we are testing the wave dark matter model against observations. Approximation 2 is a common approximation for dwarf spheroidal galaxies and is also necessary because we are comparing the wave dark matter model to the spherically symmetric Burkert mass profile. Approximation 3 seems to be consistent with observations of dwarf spheroidal galaxies at least out to large radii [6, 38]. Approximation 6 is reasonable given Figure 1. Approximations 7 and 8 are standard when modeling galaxies.

Approximations 4 and 5 are used to simplify the types of solutions to the Einstein-Klein-Gordon equations we consider. We note here, however, that there is a question of the stability of the spherically symmetric static state solutions. It is known that, if the corresponding total mass is not too large, the ground state is stable under perturbations [22, 39] but that, on their own, the excited states are not [23] regardless of their mass. However, it has also been shown that a coupling of an excited state with a ground state can produce a stable configuration [21]. We hypothesize that luminous matter distributions coupled with combinations of static states will produce a stabilizing effect allowing for more dynamically interesting systems to be physically plausible.

5. Conclusions

To summarize the results of this paper, we have drawn effectively two conclusions, which we list here.

Conclusion 5.1 *Given Approximations 1 through 8 and Rejection Criteria 3.1, if the dark matter halos of all of the eight classical dwarf spheroidal galaxies are correctly modeled by 20th excited states or less, then*

$$\Upsilon < 1000 \text{ yr}^{-1}.$$

Conclusion 5.2 *Given Approximations 1 through 8, a value of Υ which yields one or more spherically symmetric static state mass profiles which match well the best fit Burkert mass profiles computed by Salucci et al. [6] for each of the eight classical dwarf spheroidal galaxies is*

$$\Upsilon = 50 \text{ yr}^{-1}.$$

We note here that the main result of this paper is more to describe a procedure of computing a working value and upper bound of Υ rather than stating that the values that appear in the above conclusions are the best ones. If one wished to alter the hypotheses of these conclusions, the corresponding values of Υ might differ from what we presented here. However, if one remains in the realm of using static states to model the dark matter, then the procedure presented in this paper for finding an upper bound would likely still apply and could be employed to get an

upper bound under the new assumptions. As such, the conclusions above should be taken as an example of the procedure applied to a set of assumptions we currently find reasonable or useful and not as final precise estimates.

For the interested reader, the Matlab code used for this paper to generate the spherically symmetric static states and to compute the best fits to a Burkert profile can be found on Bray's Wave Dark Matter Web Page at <http://www.math.duke.edu/~bray/darkmatter/darkmatter.html>.

6. Acknowledgements

The authors gratefully acknowledge the support of National Science Foundation Grant # DMS-1007063.

References

- [1] Oort J H 1932 *Bulletin of the Astronomical Institutes of the Netherlands* **6** 249
- [2] Zwicky F 1933 *Helvetica Physica Acta* **6** 110–127
- [3] Begeman K G 1989 *Astronomy and Astrophysics* **223**(1-2) 47–60
- [4] Bosma A 1981 *The Astrophysical Journal* **86** 1791–1846 URL <http://adsabs.harvard.edu/abs/1981AJ...86.1791B>
- [5] Walker M G, Mateo M, Olszewski E W, Gnedin O Y, Wang X, Sen B and Woodroffe M 2007 *The Astrophysical Journal Letters* **667** L53 URL <http://stacks.iop.org/1538-4357/667/i=1/a=L53>
- [6] Salucci P, Wilkinson M I, Walker M G, Gilmore G F, Grebel E K, Koch A, Frigerio Martins C and Wyse R F G 2012 *Monthly Notices of the Royal Astronomical Society* **420** 2034–2041 ISSN 1365-2966 URL <http://dx.doi.org/10.1111/j.1365-2966.2011.20144.x>
- [7] Walker M G, Mateo M, Olszewski E W, Peñarrubia J, Evans N W and Gilmore G 2009 *The Astrophysical Journal* **704** 1274 URL <http://stacks.iop.org/0004-637X/704/i=2/a=1274>
- [8] Walker M G, Mateo M, Olszewski E W, Peñarrubia J, Evans N W and Gilmore G 2010 *The Astrophysical Journal* **710** 886 URL <http://stacks.iop.org/0004-637X/710/i=1/a=886>
- [9] Dahle H 2007 [*arXiv:astro-ph/0701598*] URL <http://arxiv.org/abs/astro-ph/0701598v1>
- [10] Salucci P, Martins C F and Lapi A 2010 DMAW 2010 LEGACY the Presentation Review: Dark Matter in Galaxies with its Explanatory Notes URL http://www.sissa.it/ap/dmg/dmaw_presentation.html
- [11] Hooper D and Baltz E A 2008 *Ann.Rev.Nucl.Part.Sci.* **58** 293–314
- [12] Bertone G, Hooper D and Silk J 2005 *Physics Reports* **405** 279–390 ISSN 0370-1573 URL <http://www.sciencedirect.com/science/article/pii/S0370157304003515>
- [13] Ostriker J 1993 *Annual Review of Astronomy and Astrophysics* **31** 689–716
- [14] Trimble V 1987 *Annual Review of Astronomy and Astrophysics* **25** 425–472 URL <http://www.annualreviews.org/doi/abs/10.1146/annurev.aa.25.090187.002233>
- [15] Binney J and Merrifield M 1998 *Galactic Astronomy* Princeton Series in Astrophysics (Princeton University Press)
- [16] Binney J and Tremaine S 2008 *Galactic Dynamics* Princeton Series in Astrophysics (Princeton University Press)
- [17] Bray H 2013 *AMS Contemporary Mathematics* **599** 1–64 URL <http://arxiv.org/abs/1004.4016>
- [18] Bray H 2012 [*arXiv:1212.5745 [physics.gen-ph]*] URL <http://arxiv.org/abs/1212.5745>
- [19] Lee J W 2009 *Journal of the Korean Physical Society* **54** 2622 URL <http://arxiv.org/abs/0801.1442>
- [20] Matos T, Vázquez-González A and Magaña J 2009 *Monthly Notices of the Royal Astronomical Society* **393** 1359–1369 ISSN 1365-2966 URL <http://dx.doi.org/10.1111/j.1365-2966.2008.13957.x>
- [21] Bernal A, Barranco J, Alic D and Palenzuela C 2010 *Phys. Rev. D* **81** 044031 URL <http://arxiv.org/abs/0908.2435>
- [22] Seidel E and Suen W M 1990 *Phys. Rev. D* **42**(2) 384–403 URL <http://link.aps.org/doi/10.1103/PhysRevD.42.384>
- [23] Balakrishna J, Seidel E and Suen W M 1998 *Phys. Rev. D* **58**(10) 104004 URL <http://link.aps.org/doi/10.1103/PhysRevD.58.104004>
- [24] Bernal A, Matos T and Núñez D 2008 *Revista Mexicana de Astronomía y Astrofísica* **44** 149–160 URL <http://arxiv.org/abs/astro-ph/0303455v3>
- [25] Sin S J 1994 *Phys. Rev. D* **50**(6) 3650–3654 URL <http://link.aps.org/doi/10.1103/PhysRevD.50.3650>
- [26] Schunck F and Mielke E 2003 *Classical and Quantum Gravity* **20** R301–R356 URL <http://stacks.iop.org/0264-9381/20/i=20/a=201>

- [27] Sharma R, Karmakar S and Mukherjee S 2008 [*arXiv:0812.3470 [gr-qc]*] URL <http://arxiv.org/abs/0812.3470>
- [28] Ji S U and Sin S J 1994 *Phys. Rev. D* **50**(6) 3655–3659 URL <http://link.aps.org/doi/10.1103/PhysRevD.50.3655>
- [29] Lee J W and Koh I G 1992 *Abstracts, Bulletin of the Korean Physical Society* **10**
- [30] Lee J W and Koh I G 1996 *Phys. Rev. D* **53**(4) 2236–2239 URL <http://link.aps.org/doi/10.1103/PhysRevD.53.2236>
- [31] Guzmán F S, Matos T and Villegas-Brena H 2001 *Rev. Mex. Astron. Astrofis.* **37** 63–72 URL <http://arxiv.org/abs/astro-ph/9811143>
- [32] Parry A R 2012 [*arXiv:1212.6426 [gr-qc]*] URL <http://arxiv.org/abs/1212.6426>
- [33] Burkert A 1995 *The Astrophysical Journal Letters* **447** L25 URL <http://stacks.iop.org/1538-4357/447/i=1/a=L25>
- [34] Parry A R 2014 *Analysis and Mathematical Physics* **4** 333–375 ISSN 1664-2368 URL <http://dx.doi.org/10.1007/s13324-014-0085-x>
- [35] Parry A R 2013 *Wave Dark Matter and Dwarf Spheroidal Galaxies* Ph.D. thesis Duke University URL <http://arxiv.org/abs/1311.6087>
- [36] Bizoń P and Wasserman A 2000 *Communications in Mathematical Physics* **215** 357–373 ISSN 0010-3616 URL <http://dx.doi.org/10.1007/s002200000307>
- [37] Kleya J, Wilkinson M I, Evans N W, Gilmore G and Frayn C 2002 *Monthly Notices of the Royal Astronomical Society* **330** 792–806 ISSN 1365-2966 URL <http://dx.doi.org/10.1046/j.1365-8711.2002.05155.x>
- [38] Côté P, Mateo M, Olszewski E W and Cook K H 1999 *The Astrophysical Journal* **526** 147 URL <http://stacks.iop.org/0004-637X/526/i=1/a=147>
- [39] Lai C W and Choptuik M W 2007 [*arXiv:0709.0324 [gr-qc]*] URL <http://arxiv.org/abs/0709.0324>